J. Fluid Mech. (1989), *vol.* 205, *pp.* 397–419
Printed in Great Britain

Interactions of currents and weakly nonlinear water waves in shallow water

By SUNG B. YOON† AND PHILIP L.-F. LIU
Joseph DeFrees Hydraulics Laboratory, School of Civil and Environmental Engineering, Cornell University, Ithaca, NY 14853 USA

(Received 22 March 1988 and in revised form 30 October 1988)

Two-dimensional Boussinesq-type depth-averaged equations are derived for describing the interactions of weakly nonlinear shallow-water waves with slowly varying topography and currents. The current velocity varies appreciably within a characteristic wavelength. The effects of vorticity in the current field are considered. The wave field is decomposed into Fourier time harmonics. A set of evolution equations for the wave amplitude functions of different harmonics is derived by adopting the parabolic approximation. Numerical solutions are obtained for shallow-water waves propagating over rip currents on a plane beach and an isolated vortex ring. Numerical results show that the wave diffraction and nonlinearity are important in the examples considered.

1. Introduction

The transformation of water waves over varying currents has been studied extensively by many researchers using the well-known wave-action equation (e.g. Longuet-Higgins & Stewart 1961; Bretherton & Garrett 1969; Phillips 1966). There is an excellent review on this subject by Peregrine (1976). The wave-action equation is equivalent to the geometrical ray theory and cannot be applied to the regions near caustics where wave diffraction becomes important. Local improvements have been developed for various types of caustics for both linear and nonlinear waves (McKee 1974; Peregrine & Smith 1975; Smith 1976). On the other hand, Booij (1981), Liu (1983) and Kirby (1984) have developed various parabolic wave equations based on the linearized theory. In these parabolic wave equations, the primary wave propagation direction is specified *a priori* and the wave diffraction in the lateral direction is included. Kirby (1986) extended the linear parabolic wave equation models to include the nonlinearity of the second-order Stokes waves. The Stokes wave theory, however, becomes invalid in the shallow-water region where most coastal currents (longshore and rip currents, tidal currents near an inlet or river mouth) exist.

Liu, Yoon & Kirby (1985) developed a parabolic equation model based on the Boussinesq equations for shallow-water equations. Their model has been successfully used to calculate the transformation of weakly nonlinear shallow-water waves over an uneven bottom. The effects of currents were not, however, considered in their formulation. In this paper, we shall derive a new set of Boussinesq equations for the wave motion with the effects of currents. The current velocity is assumed to be greater than the characteristic wave orbital velocity, but smaller than the wave group velocity. The lengthscale of the current variations is assumed to be longer than

† Present address: Korea Power Engineering Co. Inc., P.O. Box 631, Youngdong, Seoul, Korea.

the characteristic wavelength. Following Liu *et al.*'s (1985) approach and focusing only on the wave motion, we apply the parabolic approximation to the new Boussinesq equations. A set of nonlinear parabolic wave equations is obtained for the amplitude functions of each harmonic of the wave motion. In applying the parabolic approximation, the current velocity field is specified in such a way that the vorticity is allowed in the formulation.

In the following section, the derivation of the new Boussinesq equations are given. These equations describe the full interactions between waves and currents. Assuming that the current field is prescribed, the parabolic approximation applied to the wave field is discussed in §3. In the next section two numerical examples: rip currents on a plane beach and an isolated vortex ring, are presented. Rip currents are components of coastal current systems and could be generated by breaking waves with alongshore variations (e.g. Liu & Mei 1975). When a breakwater or a headland intercepts longshore currents and causes flow separation, the isolated vortex ring exists in the shallow water. Numerical solutions of the present model are compared with the ray pattern and the solutions from the linearized theory to illustrate the importance of the diffraction and the nonlinearity.

2. Derivation of Boussinesq equations for wave–current interactions

Peregrine (1967) derived the Boussinesq equations for shallow-water waves propagating over a varying depth by integrating the Euler's equations of motion throughout the depth. Using a perturbation method, Madsen & Mei (1969) also obtained the same set of Boussinesq equations. These equations do not, however, include the effects of currents on waves. In this section, we follow Phillips' (1966) approach, and derive a new set of Boussinesq equations which include both effects of depth variations and varying currents on waves. The magnitude of the current velocity is assumed to be stronger than that of the characteristic wave orbital velocity but weaker than that of the wave group velocity. The horizontal lengthscales of the current and the depth variations are assumed to be longer than the characteristic wavelength.

Consider a flow region bounded by a free surface $z' = \zeta'(x', t')$ and a stationary bottom, $z' = -h'(x_i')$, where x_i' $(i = 1, 2)$ are the horizontal axes and t' the time. The horizontal velocity components are denoted by $q_i'(x_i', z', t')$ $(i = 1, 2)$, while the vertical velocity component is represented by $w'(x_i', z', t')$. Choosing the inverse of a characteristic wave frequency, ω', as the timescale, a characteristic depth, h_0', as the vertical lengthscale, a characteristic wavelength, $(gh_0')^{\frac{1}{2}}/\omega'$, as the horizontal lengthscale, and a characteristic wave amplitude, a_0', as the lengthscale for the free-surface displacement, we can define the following dimensionless variables:

$$\left.\begin{aligned} t = \omega' t', \quad x_i = \frac{\omega'}{(gh_0')^{\frac{1}{2}}} x_i', \quad h = \frac{h'}{h_0'}, \quad z = \frac{z'}{h_0'}, \\ \zeta = \frac{\zeta'}{\epsilon h_0'}, \quad q_i = \frac{q_i'}{\mu (gh_0')^{\frac{1}{2}}}, \quad w = \frac{w'}{\mu\epsilon (gh_0')^{\frac{1}{2}}}, \quad p = \frac{p'}{\rho g h_0'}, \end{aligned}\right\} \tag{2.1}$$

where

$$\epsilon = \frac{a_0'}{h_0'} \ll 1, \quad \mu^2 = \frac{\omega'^2 h_0'}{g} \ll 1, \tag{2.2}$$

with p' being the pressure. Here the quantities with a prime denote the physical variables. Two small parameters, ϵ and μ^2, are the measures of nonlinearity and

frequency dispersion, and are assumed to be of same order of magnitude. The wave orbital velocity, of the order of magnitude $O(\epsilon(gh_0')^{\frac{1}{2}})$ and is, therefore, weaker than the leading-order current velocity which is $O(\mu(gh_0')^{\frac{1}{2}})$ as indicated in (2.1). The horizontal lengthscales for depth and current variations are to be specified.

The dimensionless continuity equation for an incompressible fluid flow reads:

$$\frac{1}{\mu}\frac{\partial q_i}{\partial x_i}+\frac{\partial w}{\partial z}=0, \tag{2.3}$$

where the usual summation convention over repeated indices is used. The horizontal and the vertical momentum equations can be expressed in the following dimensionless forms:

$$\left.\begin{aligned}&\frac{\partial q_j}{\partial t}+\mu\frac{\partial q_i q_j}{\partial x_i}+\epsilon\frac{\partial q_j w}{\partial z}+\frac{1}{\mu}\frac{\partial p}{\partial x_j}=0 &(2.4)\\ &\frac{\partial w}{\partial t}+\mu\frac{\partial q_i w}{\partial x_i}+\epsilon\frac{\partial w^2}{\partial z}+\frac{1}{\mu^2\epsilon}\frac{\partial p}{\partial z}+\frac{1}{\epsilon\mu^2}=0 &(2.5)\end{aligned}\right\}\quad (j=1,2).$$

On the free surface, $z=\epsilon\zeta$, the kinematic boundary condition requires

$$\frac{\partial\zeta}{\partial t}+\mu q_i\frac{\partial\zeta}{\partial x_i}-w=0,\quad z=\epsilon\zeta. \tag{2.6}$$

The dynamic condition demands the continuity of the pressure across the free surface. It is assumed that

$$p=0,\quad z=\epsilon\zeta. \tag{2.7}$$

Along the rigid bottom, $z=-h$, the no-flux boundary condition is used. Thus

$$q_i\frac{\partial h}{\partial x_i}+\mu w=0,\quad z=-h. \tag{2.8}$$

In the present analysis the current field is allowed to be rotational. However, the horizontal velocity components are almost uniform throughout the depth. The vertical vorticity components are required to satisfy the following condition:

$$\frac{\partial q_i}{\partial z}-\mu\epsilon\frac{\partial w}{\partial x_i}=O(\mu^2\epsilon,\mu^4)\quad (i=1,2) \tag{2.9}$$

Following Phillips' (1966) approach, we integrate the continuity equation, (2.3), and the horizontal momentum equations, (2.4), from the bottom to the free surface to get

$$\frac{\partial\zeta}{\partial t}+\frac{1}{\mu}\frac{\partial}{\partial x_i}\int_{-h}^{\epsilon\zeta}q_i\,\mathrm{d}z=0, \tag{2.10}$$

$$\frac{\partial}{\partial t}\int_{-h}^{\epsilon\zeta}q_j\,\mathrm{d}z+\mu\frac{\partial}{\partial x_i}\int_{-h}^{\epsilon\zeta}q_i q_j\,\mathrm{d}z+\frac{1}{\mu}\frac{\partial}{\partial x_j}\int_{-h}^{\epsilon\zeta}p\,\mathrm{d}z-\frac{1}{\mu}[p]_{-h}\frac{\partial h}{\partial x_j}=0, \tag{2.11}$$

in which $i,j=1,2$ and the boundary conditions (2.6)–(2.8) have been employed. The pressure field can be obtained by integrating the vertical momentum equation, (2.5),

$$[p]=\epsilon\zeta-z+\epsilon\mu^2\frac{\partial}{\partial t}\int_z^{\epsilon\zeta}w\,\mathrm{d}z+\epsilon^2\mu\frac{\partial}{\partial x_i}\int_z^{\epsilon\zeta}q_i w\,\mathrm{d}z-\epsilon^2\mu^2[w^2]_z. \tag{2.12}$$

The free-surface boundary conditions have been used in the integration. Similarly,

the vertical velocity component at a certain water depth can be obtained by integrating the continuity equation, (2.3), from $z = -h$ to z. Thus

$$[w]_z = -\frac{1}{\mu}\frac{\partial}{\partial x_i}\int_{-h}^{z} q_i \,\mathrm{d}z, \tag{2.13}$$

in which the bottom boundary condition, (2.8), has been applied.

Up to this point, no approximation has been used in obtaining the vertically integrated equations, (2.7)–(2.13). These equations are exact. The details of the integration procedures can be found in Phillips (1966), Liu & Mei (1975) and Yoon (1987). In these earlier works, scales for the velocity field are different from those specified in (2.1). The coefficients, in terms of small parameters, in the resulting equations are different from the present equations. The integration procedures and the forms of the resulting equations remain the same.

To proceed to further analysis, several approximations and simplifications are adopted. The velocity field is assumed to consist of a slowly time-varying current velocity component and a fluctuating wave component. The current velocity is of the magnitude of $O(\mu(gh_0')^{\frac{1}{2}})$, but the wave orbital velocity is of $O(\epsilon(gh_0')^{\frac{1}{2}})$. Denoting by $\bar{q}_i$ the horizontal components of the current velocity and $\tilde{q}_i$ the horizontal components of the wave orbital velocity, we can decompose the velocity field as

$$q_i = \bar{q}_i + \frac{\epsilon}{\mu}\tilde{q}_i. \tag{2.14}$$

The corresponding free-surface displacements can be written as

$$\zeta = \frac{\mu^2}{\epsilon}\bar{\zeta} + \tilde{\zeta}. \tag{2.15}$$

We further assume that the lengthscale of the depth variations as well as of the current variations is longer than the characteristic wavelength. Thus

$$O\left(\frac{\partial h}{\partial x_i}\right) \sim O\left(\frac{\partial \bar{q}_i}{\partial x_i}\right) \sim O\left(\frac{\partial \bar{\zeta}}{\partial x_i}\right) \sim O(\mu). \tag{2.16a}$$

The current field varies slowly in time, i.e.

$$O\left(\frac{\partial \bar{q}_i}{\partial t}\right) \sim O\left(\frac{\partial \bar{\zeta}}{\partial t}\right) \sim O(\mu^2). \tag{2.16b}$$

Applying the order of magnitude arguments, (2.14) and (2.16a), in the continuity equation, (2.3), we find that the dimensionless vertical velocity component, w, is indeed of $O(1)$. Invoking the irrotationality condition, (2.9), we determine that the horizontal velocity components are uniform throughout the entire depth up to $O(\mu^2, \epsilon)$, i.e.

$$q_i(x_i, z, t) = q_i^*(x_i, t) + O(\mu\epsilon, \mu^3), \tag{2.17}$$

where q_i^* can be viewed as the horizontal velocity components on the free surface. Substituting (2.17) into (2.13), we find that the approximate vertical velocity component is

$$[w]_z = -\frac{z}{\mu}\frac{\partial q_i^*}{\partial x_i} - \frac{1}{\mu}\frac{\partial h q_i^*}{\partial x_i} + O(\epsilon, \mu^2). \tag{2.18}$$

Similarly, the pressure field, (2.12) can be approximated as

$$[p]_z = \epsilon\zeta - z + \epsilon\mu^2 \frac{\partial}{\partial t}\int_z^0 w\,\mathrm{d}z + \epsilon^2\mu \frac{\partial}{\partial x_i}\int_z^0 q_i\, w\,\mathrm{d}z + O(\mu^6, \epsilon^2\mu^2).$$

Substitutions of (2.17) and (2.18) into the equation above lead to

$$[p]_z = (\epsilon\zeta - z) + \epsilon\mu\left[\tfrac{1}{2}z^2 \frac{\partial}{\partial x_i}\left(\frac{\partial q_i^*}{\partial t}\right) + z\frac{\partial}{\partial x_i}\left(h\frac{\partial q_i^*}{\partial t}\right)\right] + \epsilon^2\left[\frac{z^2}{2}\frac{\partial}{\partial x_i}\left(q_i^*\frac{\partial q_k^*}{\partial x_k}\right) + z\frac{\partial}{\partial x_i}\left(q_i^*\frac{\partial h q_k^*}{\partial x_k}\right)\right] + O(\mu^6, \epsilon^2\mu^2). \quad (2.19)$$

The approximated horizontal velocity components can be obtained by integrating (2.9) from $z = z$ to $z = \epsilon\zeta$, i.e.

$$[q_i]_z = q_i^* - \mu\epsilon\int_z^0 \frac{\partial w}{\partial x_i}\mathrm{d}z + O(\mu\epsilon^2)$$

$$= q_i^* - \epsilon\left[\tfrac{1}{2}z^2\frac{\partial}{\partial x_i}\frac{\partial q_k^*}{\partial x_k} + z\frac{\partial}{\partial x_i}\frac{\partial (q_k^* h)}{\partial x_k}\right] + O(\mu\epsilon^2), \quad (2.20)$$

in which (2.18) has been employed.

Now we introduce the depth-averaged horizontal velocity components as

$$u_i = \frac{1}{h+\epsilon\zeta}\int_{-h}^{\epsilon\zeta} q_i\,\mathrm{d}z \quad (i = 1, 2). \quad (2.21)$$

The relationship between the depth-averaged velocity, u_i, and the free-surface velocity, q_i^*, can be found by substituting (2.20) into (2.21). Thus

$$u_i = q_i^* - \tfrac{1}{6}\epsilon h^2 \frac{\partial}{\partial x_i}\frac{\partial q_k^*}{\partial x_k} + \tfrac{1}{2}\epsilon h\frac{\partial}{\partial x_i}\frac{\partial q_k^* h}{\partial x_k} + O(\mu^5, \mu\epsilon^2). \quad (2.22)$$

Finally, using (2.19)–(2.22), we can rewrite the continuity equation, (2.10) and the momentum equation, (2.11), in terms of the depth-averaged velocity, u_i, in the following forms:

$$\frac{\partial\zeta}{\partial t} + \frac{1}{\mu}\frac{\partial}{\partial x_i}[(h+\epsilon\zeta)\,u_i] = 0, \quad (2.23)$$

$$\frac{\partial}{\partial t}[(h+\epsilon\zeta)\,u_j] + \mu\frac{\partial}{\partial x_i}[(h+\epsilon\zeta)\,u_i u_j] + \frac{\epsilon}{\mu}(h+\epsilon\zeta)\frac{\partial\zeta}{\partial x_j} + \epsilon\left[\tfrac{1}{6}h^3\frac{\partial}{\partial x_j}\frac{\partial}{\partial x_i}\left(\frac{\partial q_i^*}{\partial t}\right)\right.$$

$$\left. - \tfrac{1}{2}h^2\frac{\partial}{\partial x_j}\frac{\partial}{\partial x_i}\left(h\frac{\partial q_i^*}{\partial t}\right)\right] - \frac{\epsilon^2}{\mu}\tfrac{1}{3}h^3\frac{\partial}{\partial x_j}\frac{\partial}{\partial x_i}\left(q_i^*\frac{\partial q_k^*}{\partial x_k}\right) = O(\mu^5) \quad (i, j = 1, 2). \quad (2.24)$$

While the continuity equation, (2.23), remains exact, the momentum equations, (2.24), are approximated.

Similarly to (2.14) and (2.15), we decompose the depth-averaged horizontal velocity components and the free-surface displacement into the current component and the wave component, i.e.

$$u_i = u_{ci} + \frac{\epsilon}{\mu}u_{wi}, \quad (2.25)$$

$$\zeta = \frac{\mu^2}{\epsilon}\zeta_c + \zeta_w, \quad (2.26)$$

where the subscripts c and w denote the current component and the wave component, respectively. The current components are the remainders of the time average of u_i and ζ over a wave period. Substituting (2.25) and (2.26) into the continuity equation, (2.23), and taking a time average over a wave period, we obtain

$$\frac{\partial \zeta_c}{\partial t}+\frac{\partial}{\partial x_i}\left[\frac{\mu}{\epsilon}(h+\mu^2\zeta_c)\,u_{ci}+\epsilon\langle\zeta_w\,u_{wi}\rangle\right]=0, \tag{2.27}$$

in which $\langle\ \rangle$ represents the time average. The term $\langle\zeta_w\,u_{wi}\rangle$ is the Eulerian mass transport velocity component due to wave fluctuations. It is convenient for some problems to introduce the total current field velocity including the mass transport, i.e.

$$u_{ti}=u_{ci}+\frac{\epsilon^2}{\mu}\frac{\langle\zeta_w\,u_{wi}\rangle}{(h+\mu^2\zeta_c)}. \tag{2.28}$$

The continuity equation, (2.27), can be rewritten in terms of u_{ti} as

$$\frac{\partial \zeta_c}{\partial t}+\frac{\mu}{\epsilon}\frac{\partial}{\partial x_i}[Du_{ti}]=0, \tag{2.29}$$

where $D=h+\mu^2\zeta_c$ is the total mean depth.

The momentum equations for the total current field can be obtained from (2.4) after taking the time average. Thus

$$\frac{\partial}{\partial t}[Du_{tj}]+\mu\frac{\partial}{\partial x_i}[Du_{ti}u_{tj}]+\mu D\frac{\partial \zeta_c}{\partial x_j}+\frac{\epsilon^2}{\mu}\frac{\partial S_{ij}}{\partial x_i}=O(\mu^5), \tag{2.30}$$

where

$$S_{ij}=h\langle u_{wi}\,u_{wj}\rangle+\tfrac{1}{2}\langle\zeta_w^2\rangle\,\delta_{ij}, \tag{2.30}$$

is the radiation stress tensor first given by Longuet-Higgins & Stewart (1960) and δ_{ij} is the Kronecker Delta function. Equation (2.30) can be further simplified, when (2.29) is used. Hence,

$$\frac{\partial u_{tj}}{\partial t}+\mu u_{ti}\frac{\partial u_{tj}}{\partial x_i}+\mu\frac{\partial \zeta_c}{\partial x_j}+\frac{\epsilon^2}{\mu D}\frac{\partial S_{ij}}{\partial x_i}=O(\mu^5). \tag{2.31}$$

The time- and depth-averaged continuity equation and momentum equations are essentially the same as those derived by Phillips (1966) and Liu & Mei (1975). The present equations are, however, obtained specifically for shallow-water waves.

Subtracting the time- and depth-averaged equation, (2.29), and the momentum equations, (2.30), from (2.23) and (2.24), respectively, we obtain the corresponding continuity equation and momentum equations for the wave (fluctuation) components:

$$\frac{\partial \zeta_w}{\partial t}+\frac{\partial}{\partial x_i}[(D+\epsilon\zeta_w)\,u_{wi}+\mu\zeta_w\,u_{ci}-\epsilon\langle\zeta_w\,u_{wi}\rangle]=0 \quad (i=1,2) \tag{2.32}$$

$$\begin{aligned}&\frac{\partial u_{wj}}{\partial t}+\mu u_{ci}\frac{\partial u_{wj}}{\partial x_i}+\mu u_{wi}\frac{\partial u_{cj}}{\partial x_i}+\epsilon u_{wi}\frac{\partial u_{wj}}{\partial x_i}-\epsilon\left\langle u_{wi}\frac{\partial u_{wj}}{\partial x_i}\right\rangle\\&\quad+\frac{\partial \zeta_w}{\partial x_j}-\mu^2\tfrac{1}{2}h\frac{\partial}{\partial x_j}\left[\frac{\partial}{\partial x_i}\left(h\frac{\partial u_{wi}}{\partial t}\right)\right]+\mu^2\tfrac{1}{6}h^2\frac{\partial}{\partial x_j}\left[\frac{\partial}{\partial x_i}\left(\frac{\partial u_{wi}}{\partial t}\right)\right]\\&\quad+\mu^3\tfrac{1}{3}h^2\frac{\partial}{\partial x_j}\left[u_{ci}\frac{\partial}{\partial x_i}\left(\frac{\partial u_{wk}}{\partial x_k}\right)\right]=O(\mu^4)\quad(i,j,k=1,2).\end{aligned} \tag{2.33}$$

Equations (2.32) and (2.33) represent a new set of Boussinesq equations for wave

motion including the effects of currents. If the current velocity vanishes, the above equations reduce to Peregrine's (1967) Boussinesq equations.

The governing equations for the current field and the wave field, (2.29), (2.31), (2.32) and (2.33), are coupled, The coupling is, however, rather weak. From the time- and depth-averaged momentum equation, (2.31), the wave-induced mean currents resulting from the radiation stresses are $O(\epsilon, \mu^2)$, since both the current velocity and the radiation stresses are slowly varying functions in x_i. These wave-induced mean currents affect the wave field through the inertia term in the momentum equation, i.e. the second term in (2.33). Because the inertia term is linear in u_{ci}, the modifications of wave-induced currents to the wave field are equivalent to the Doppler-shift effects. The complete solutions of the coupled system can be obtained, in principle, by an iterative numerical scheme. The first step of the iterative scheme is to calculate the current field without considering the effect of the wave field, i.e. ignoring the radiation stresses. The computed current velocity field is then used in (2.32) and (2.33) to find the wave field. The current field can be updated by re-solving (2.29) and (2.31) with the effects of the wave field. The wave field can also be updated if we solve (2.32) and (2.33) again with the new current field. The procedure can be repeated until the converged solutions are obtained. Some preliminary numerical results of this kind have been reported by Yoon (1987).

As pointed out by Yoon (1987) and others, the task of solving the current field including the effects of radiation stresses is by no means a trivial exercise. In this paper, we focus our attention on the solutions of the wave field over a prescribed current velocity field. Retaining all terms in (2.32) and (2.33) allows one to examine the refraction and diffraction of weakly nonlinear waves over a shear current. The solution technique for (2.32) and (2.33) can also be used as a module in the iterative scheme for the complete wave–current interactions.

3. Nonlinear mild-slope equations and parabolic approximation

In the remainder of this paper, we further simplify the situation by assuming that the current field is steady state and the lengthscale of the depth variations is longer than that of the current variations, i.e. $O(|\nabla h|) \sim O(\mu^2)$. Moreover, for convenience of presentation, vector notation will be used. The horizontal coordinates (x, y) replace (x_1, x_2) and the horizontal gradient is, therefore, defined as $\nabla = (\partial/\partial x_1, \partial/\partial x_2) = (\partial/\partial x, \partial/\partial y)$. The continuity equation and momentum equations for the wave field, (2.32) and (2.33) can be rewritten as

$$\frac{\partial \zeta_w}{\partial t} + \nabla \cdot [(D + \epsilon\zeta_w)\, \boldsymbol{u}_w + \mu\zeta_w \boldsymbol{u}_c - \epsilon\langle \zeta_w \boldsymbol{u}_w \rangle] = O(\mu^4), \tag{3.1}$$

$$\frac{\partial \boldsymbol{u}_w}{\partial t} + \mu \boldsymbol{u}_c \cdot \nabla \boldsymbol{u}_w + \mu \boldsymbol{u}_w \cdot \nabla \boldsymbol{u}_c + \epsilon \boldsymbol{u}_w \cdot \nabla \boldsymbol{u}_w - \epsilon \langle \boldsymbol{u}_w \cdot \nabla \boldsymbol{u}_w \rangle + \nabla \zeta_w - \tfrac{1}{3}\mu^2 D^2 \nabla \left[\frac{\partial}{\partial t} (\nabla \cdot \boldsymbol{u}_w) + \mu \boldsymbol{u}_c \cdot \nabla (\nabla \cdot \boldsymbol{u}_w \right] = O(\mu^4). \tag{3.2}$$

Note that in (3.2) D replaces h.

Consider the wave field which is periodic in time. The velocity vector and the free-surface displacement can be expressed as

$$\left.\begin{aligned} \boldsymbol{u}_w &= \tfrac{1}{2} \sum_n \boldsymbol{u}_n(\boldsymbol{x})\, e^{-int}, \quad n = \pm 1, \pm 2, \ldots, \\ \zeta_w &= \tfrac{1}{2} \sum_n \zeta_n(\boldsymbol{x})\, e^{-int}, \quad n = \pm 1, \pm 2, \ldots, \end{aligned}\right\} \tag{3.3}$$

where $(\zeta_{-n}, \boldsymbol{u}_{-n})$ is the complex conjugate of $(\zeta_n, \boldsymbol{u}_n)$. The zeroth component ($n = 0$) is not included in (3.3) because it has been accounted for in the mean current field. Substituting (3.3) into (3.1) and (3.2) and collecting the different Fourier harmonics, we obtain for the nth harmonic:

$$-in\zeta_n + \nabla\cdot(D\boldsymbol{u}_n) + \mu\nabla\cdot(\zeta_n \boldsymbol{u}_t) + \tfrac{1}{2}\epsilon \sum_{s\neq n} \nabla\cdot(\zeta_s \boldsymbol{u}_{n-s}) = O(\mu^4), \tag{3.4}$$

$$-in\boldsymbol{u}_n + \nabla\zeta_n + \mu(\boldsymbol{u}_t\cdot\nabla\boldsymbol{u}_n + \boldsymbol{u}_n\cdot\nabla\boldsymbol{u}_t) + \tfrac{1}{2}\epsilon \sum_{s\neq n} \boldsymbol{u}_s\cdot\nabla\boldsymbol{u}_{n-s}$$
$$+ in\mu^2\tfrac{1}{3}D^2\nabla(\nabla\cdot\boldsymbol{u}_n) - \tfrac{1}{3}\mu^3 D^2\nabla[\boldsymbol{u}_t\cdot\nabla(\nabla\cdot\boldsymbol{u}_n)] = O(\mu^4), \tag{3.5}$$

where $n = \pm 1, \pm 2, \ldots$, and $s = \pm 1, \pm 2, \ldots$. Multiplying (3.5) by D and taking the divergence of the resulting equation, we can combine (3.4) and (3.5) to get

$$\nabla\cdot(D\nabla\zeta_n) + n^2\zeta_n + in\mu(\nabla\cdot\boldsymbol{u}_t)\zeta_n + in\mu\nabla\zeta_n\cdot\boldsymbol{u}_t$$
$$-\tfrac{1}{3}\mu^2 n^2 D^2\nabla^2\zeta_n - 2in\mu^3\tfrac{1}{3}D^2\nabla^2(\boldsymbol{u}_t\cdot\nabla\zeta_n) + \mu\nabla\cdot[D(\boldsymbol{u}_t\cdot\nabla\boldsymbol{u}_n + \boldsymbol{u}_n\cdot\nabla\boldsymbol{u}_t)]$$
$$+\tfrac{1}{2}\epsilon \sum_{s\neq n} [D\nabla\cdot(\boldsymbol{u}_s\cdot\nabla\boldsymbol{u}_{n-s}) + in\nabla\cdot(\zeta_s \boldsymbol{u}_{n-s})] = O(\mu^4). \tag{3.6}$$

Denoting by (U, V) the total velocity components in the x- and y-direction, and assuming that the primary wave propagation direction coincides with the x-axis, we are interested in the shear current field so that

$$O\left(\frac{\partial U}{\partial y}\right) \sim O\left(\frac{\partial V}{\partial x}\right) \sim O(\mu), \tag{3.7}$$

$$O\left(\frac{\partial U}{\partial x}\right) \sim O\left(\frac{\partial V}{\partial y}\right) \sim O(\mu^2, \epsilon). \tag{3.8}$$

The lengthscales for the current velocity components given in (3.7) are the same as those specified in the original derivation, i.e. (2.16a). On the other hand, the lengthscales shown in (3.8) are required for the purpose of adopting the parabolic approximation. Because the primary wave propagation direction is in the x-direction, the lengthscale of ζ_n in the x-direction is the characteristic wavelength, while the free-surface variation in the y-direction must be slowly varying:

$$O\left(\frac{\partial \zeta_n}{\partial y}\right) \sim O(\mu), \quad O\left(\frac{\partial^2 \zeta_n}{\partial y^2}\right) \sim O(\mu^2). \tag{3.9}$$

Using (3.7), (3.8) and (3.9), one can simplify (3.6) to give

$$D\frac{\partial^2\zeta_n}{\partial x^2} + D\left(1 + \frac{\mu U}{D^{\frac{1}{2}}}\right)\frac{\partial^2\zeta_n}{\partial y^2} + \left(i\mu n D + \frac{\partial D}{\partial x}\right)\frac{\partial\zeta_n}{\partial x}$$
$$+\left[\frac{\partial D}{\partial y} + 2i\mu n V + 2\mu D^{\frac{1}{2}}\left(\frac{\partial V}{\partial x} + \frac{\partial U}{\partial y}\right)\right]\frac{\partial\zeta_n}{\partial y} - \frac{i\mu D}{n}U\frac{\partial^3\zeta_n}{\partial x^3}$$
$$+\left[n^2 + 2i\mu n\frac{\partial U}{\partial x} - 2i\mu n\frac{V}{D}\frac{\partial D}{\partial y} + \tfrac{1}{3}\mu^2 n^4 D\left(1 - \frac{4\mu V}{D^{\frac{1}{2}}}\right)\right.$$
$$\left.-i\mu^2 n\frac{V}{D^{\frac{1}{2}}}\frac{\partial U}{\partial y} - \mu^2 n^2\frac{U^2}{D}\left(1 - \frac{4\mu U}{D^{\frac{1}{2}}}\right)\right]\zeta_n = \frac{\epsilon}{2D}\sum_{s\neq n}\left[n(n+s)\right.$$
$$\left.-\frac{\mu U}{D^{\frac{1}{2}}}n(n+2s)\right]\zeta_n\,\zeta_{n-s} + O(\mu^4), \tag{3.10}$$

which can be considered as a nonlinear mild-slope equation for the nth harmonic. To solve the above equation one must prescribe the boundary conditions along the boundaries. Furthermore, since the lengthscale of variation of ζ_n is a typical wavelength, the required numerical discretization and computations might be costly. The alternative is to make further approximation and to rewrite (3.10) in a parabolic equation form.

Consider a slowly varying amplitude function ψ_n such that

$$\zeta_n = \psi_n(x, y)\, \mathrm{e}^{\mathrm{i}n \int d^{-\frac{1}{2}} \mathrm{d}x}, \tag{3.11}$$

where $d(x)$ is a reference depth varying slowly in the x-direction. $O(\nabla h) \sim O(\mu^2)$ and, from (3.7) and (3.8), the amplitude function, ψ_n, varies faster in the y-direction than in the x-direction. Thus, the usual parabolic approximations are adopted:

$$\left.\begin{aligned} &O\left(\frac{\partial \psi_n}{\partial y}\right) \sim O(\mu), \quad \frac{\partial^2 \psi_n}{\partial y^2} \sim O(\mu^2), \\ &O\left(\frac{\partial \psi_n}{\partial y}\right) \sim O(\mu^2), \quad \frac{\partial^2 \psi_n}{\partial x^2} \sim O(\mu^4), \quad \frac{\partial^3 \psi_n}{\partial x^3} \sim O(\mu^6). \end{aligned}\right\} \tag{3.12}$$

Substituting (3.11) and (3.12) into (3.10) and keeping all the terms up to $O(\mu^3)$, one obtains

$$\begin{aligned} &2\mathrm{i}n\left(\frac{D}{d^{\frac{1}{2}}} + 2\mu U\right)\frac{\partial \psi_n}{\partial x} + D\left(1 + \frac{\mu U}{D^{\frac{1}{2}}}\right)\frac{\partial^2 \psi_n}{\partial y^2} + \left[\frac{\partial D}{\partial y} + 2\mathrm{i}\mu n V + 2\mu D^{\frac{1}{2}}\right. \\ &\left.\times\left(\frac{\partial V}{\partial x} + \frac{\partial U}{\partial y}\right)\right]\frac{\partial \psi_n}{\partial y} + \left\{\mathrm{i}n\frac{\partial}{\partial x}\left(\frac{D}{d^{\frac{1}{2}}} + 2\mu U\right) + n^2\left[1 - \frac{D}{d} - \mu\frac{U}{d^{\frac{1}{2}}}\left(1 + \frac{D}{d}\right)\right.\right. \\ &\left.\left. + \tfrac{1}{3}\mu^2 n^2 D\left(1 - \frac{4\mu U}{D^{\frac{1}{2}}}\right) - \frac{\mu^2 U^2}{D}\left(1 - \frac{4\mu U}{D^{\frac{1}{2}}}\right)\right] - 2\mathrm{i}\mu n\frac{V}{D}\frac{\partial D}{\partial y} - \mathrm{i}\mu^2 n\frac{V}{D^{\frac{1}{2}}}\frac{\partial U}{\partial y}\right. \\ &\left. - \tfrac{3}{4}\mathrm{i}\mu n\frac{U}{d^{\frac{1}{2}}}\frac{\partial d}{\partial x}\right\}\psi_n = \frac{\epsilon}{2D}\sum_{s \neq n}\left[n(n+s) - \frac{\mu U}{D^{\frac{1}{2}}}n(n+2s)\right]\psi_s \psi_{n-s} + O(\mu^4), \end{aligned} \tag{3.13}$$

where $D/d = 1 + \mathrm{O}(\mu^2)$ has been employed. The above equation is a parabolic wave equation describing the wave propagation over a varying current and a varying depth.

If the effects of current field are ignored, (3.13) can be simplified to

$$\begin{aligned} &2\mathrm{i}n\frac{h}{d^{\frac{1}{2}}}\frac{\partial \psi_n}{\partial x} + h\frac{\partial^2 \psi_n}{\partial y^2} + \frac{\partial h}{\partial y}\frac{\partial \psi_n}{\partial y} + \left\{\mathrm{i}n\frac{\partial}{\partial x}\left(\frac{h}{d^{\frac{1}{2}}}\right)\right. \\ &\left. + n^2\left(1 - \frac{h}{d} + \tfrac{1}{3}\mu^2 n^2 h\right)\right\}\psi_n = \frac{\epsilon}{2h}\sum_{s \neq n} n(n+s)\,\psi_s \psi_{n-s} + O(\mu^4), \end{aligned} \tag{3.14}$$

which has also been derived by Liu *et al.* (1985).

4. Numerical examples

To find numerical solutions for the wave field, the Crank–Nicolson method is used to rewrite (3.13) in a finite-difference form. The forward-difference is used in the x-direction and the centred-difference is used in the y-direction. Denoting $\psi^j_{n,k}$ as the nth harmonic amplitude function at $x (= j\Delta x)$ and $y (= k\Delta y)$, we can rewrite (3.13) in the following form:

$$2in\left(\frac{D}{d^{\frac{1}{2}}}+2\mu U\right)_k^{j+1}\frac{\psi_{n,k}^{j+1}-\psi_{n,k}^{j}}{\Delta x}+D_k^{j+1}\left(1+\frac{\mu U}{D^{\frac{1}{2}}}\right)_k^{j+1}\frac{\delta^2\psi_{n,k}^{j+1}+\delta^2\psi_{n,k}^{j}}{2\Delta y^2}$$

$$+\left[\frac{\delta D_k^{j+1}}{2\Delta y}+2i\mu nV_k^{j+1}+2\mu(D_k^{j+1})^{\frac{1}{2}}\left(\frac{V_k^{j+1}-V_k^{j}}{\Delta x}+\frac{\delta U_k^{j+1}}{2\Delta y}\right)\right]$$

$$\times\frac{\delta\psi_{n,k}^{j+1}+\delta\psi_{n,k}^{j}}{4\Delta y}+\left\{\frac{in}{\Delta x}\left[\left(\frac{D}{d^{\frac{1}{2}}}+2\mu U\right)_k^{j+1}-\left(\frac{D}{d^{\frac{1}{2}}}+2\mu U\right)_k^{j}\right]+n^2\right.$$

$$\times\left[1-\left(\frac{D}{d^{\frac{1}{2}}}\right)_k^{j+1}+\mu\left(\frac{U}{d^{\frac{1}{2}}}\right)_k^{j+1}\left(1+\frac{D}{d^{\frac{1}{2}}}\right)_k^{j+1}+\tfrac{1}{3}\mu^2n^2D_k^{j+1}\left(1-\frac{4\mu U}{D^{\frac{1}{2}}}\right)_k^{j+1}\right.$$

$$\left.-\mu^2\left(\frac{U^2}{D}\right)_k^{j+1}\left(1-\frac{4\mu U}{D^{\frac{1}{2}}}\right)_k^{j+1}\right]-2i\mu n\left(\frac{V}{D}\right)_k^{j+1}\frac{\delta D_k^{j+1}}{2\Delta y}$$

$$\left.-i\mu^2n\left(\frac{V}{D^{\frac{1}{2}}}\right)_k^{j+1}\frac{\delta U_k^{j+1}}{2\Delta y}-\tfrac{3}{4}i\mu n\left(\frac{U}{d^{\frac{1}{2}}}\right)_k^{j+1}\frac{d_k^{j+1}-d_k^{j}}{\Delta x}\right\}\tfrac{1}{2}(\psi_{n,k}^{j+1}+\psi_{n,k}^{j})$$

$$=\frac{\epsilon}{4D_k^{j+1}}\sum_{s\neq n}\left[n(n+s)-\mu\left(\frac{U}{D^{\frac{1}{2}}}\right)_k^{j+1}n(n+2s)\right](\psi_{s,k}^{j+1}\psi_{n-s,k}^{j+1}+\psi_{s,k}^{j}\psi_{n-s,k}^{j}),\qquad(4.1)$$

where
$$\delta(\,)_k=(\,)_{k+1}-(\,)_{k-1},\quad \delta^2(\,)_k=(\,)_{k+1}-2(\,)_k+(\,)_{k-1}.\qquad(4.2a,b)$$

The right-hand side of (4.1) is nonlinear and has been linearized for computational purposes in the following way:

$$\psi_{s,k}^{j+1}\psi_{n-s,k}^{j+1}=(\psi_{s,k}^{j+1})^m(\psi_{n-s,k}^{j+1})^{m+1},\qquad(4.3)$$

where the superscript m denotes the number of iterations. The initial guesses, $m=0$, are obtained from the previous x-level solutions, i.e. $(\psi_{s,k}^{j+1})^0=\psi_{s,k}^{j}$. The iteration process is stopped and the converged solution is obtained if the relative error is less than a predetermined small number, i.e.

$$\frac{|(\psi_{n,k}^{j+1})^{m+1}-(\psi_{n,k}^{j+1})^m|}{|(\psi_{n,k}^{j+1})^m|}<10^{-4}.\qquad(4.4)$$

Equation (4.1) results in an asymmetrical banded matrix with a band width $2N+1$, where N is the total number of harmonics used in computations. The Crank–Nicolson method is unconditionally stable for the linear version of (4.1). The method seems to be free of stability problems for the nonlinear problems studied here.

Numerical resuts are obtained for the refraction and diffraction of cnoidal waves over two different current fields: rip currents on a uniform slope and an isolated vortex ring on a constant depth. In both cases, the current velocity is prescribed; the effects of waves on current are not taken into account.

4.1. *Rip currents*

Arthur (1950) studied wave propagation over rip (jet-like) currents using a linear wave ray theory. Because of wave refraction, wave ray crossings occur along the centreline of the rip currents. The ray theory becomes invalid in the neighbourhood of wave crossings. In this section, we re-examine Arthur's wave–current interaction problems by using the nonlinear parabolic equations, (3.13). The effects of the current strength and the lengthscales of current variations on waves are investigated.

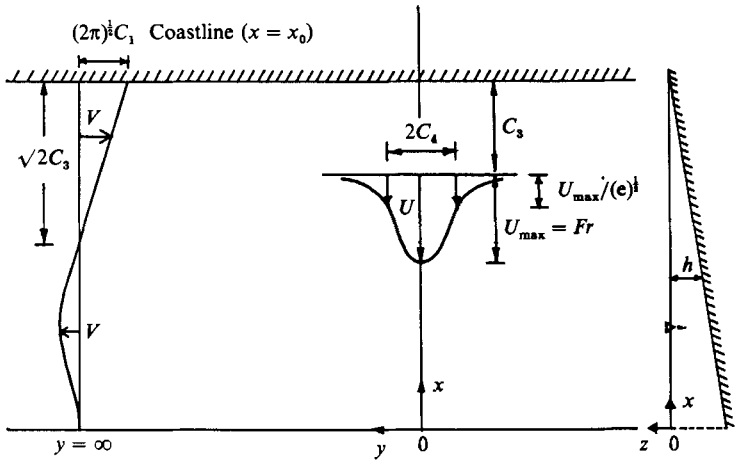

FIGURE 1. Definition sketch of Arthur's (1950) rip current.

Case	Fr	C_4	ϵ	μ^2
1	0.1177	0.798	0.01	0.361
2	0.1177	0.798	0.02	0.361
3	0.2353	0.798	0.01	0.361
4	0.2353	0.798	0.02	0.361
5	0.2353	1.596	0.01	0.361
6	0.2353	1.596	0.02	0.361

TABLE 1. Parameters for each rip currents

Arthur's (1950) rip current velocity components can be recast in the following dimensionless form:

$$U = -C_2(x_0 - x)\,\mathrm{e}^{-\alpha^2/2}\,\mathrm{e}^{-\beta^2/2}, \tag{4.5a}$$

$$V = -(\tfrac{1}{2}\pi)^{\frac{1}{2}}C_1(2-\alpha^2)\,\mathrm{e}^{-\alpha^2/2}\,\mathrm{erf}\,(\beta/\sqrt{2}), \tag{4.5b}$$

where

$$C_1 = \frac{C_4\,\mathrm{e}^{\frac{1}{2}}}{C_3}Fr, \quad C_2 = \frac{C_1}{C_4}, \quad Fr = \frac{\max(U')}{\mu(gh_0')^{\frac{1}{2}}}, \quad \alpha = \frac{x_0 - x}{C_3}, \quad \beta = \frac{y}{C_4}, \tag{4.5c}$$

and $x = x_0$ is the location of the coastline. The bottom topography is a uniform beach and can be expressed as

$$h = (x_0 - x)/x_0. \tag{4.5d}$$

In Arthur's study, the beach slope is fixed as $s = h_0'/x_0' = 1/50$. Note that Arthur's current velocity field satisfies only the continuity equation with $\zeta_c = 0$.

As shown in figure 1, the tip current pattern is determined by three parameters: Fr, C_3 and C_4. The strength of the tip current is controlled by the Froude number Fr, while C_3 gives the location of the on–offshore maximum velocity and C_4 governs the width of the rip current. In our numerical computations, C_3 is fixed at 7.979 and six different combinations of parameters are used. These parameters are listed in table 1. The rip current velocity reported in Arthur's paper corresponds to $Fr = 0.2353$, $C_4 = 0.798$ and $C_3 = 7.979$. We remark here that for all cases the computed maximum current velocity is smaller than the shallow-water phase velocity and the width of the rip currents is of the same order of magnitude as a typical wavelength. Along the initial (offshore) phaseline the nonlinearity parameter, ϵ, is one order smaller than μ^2.

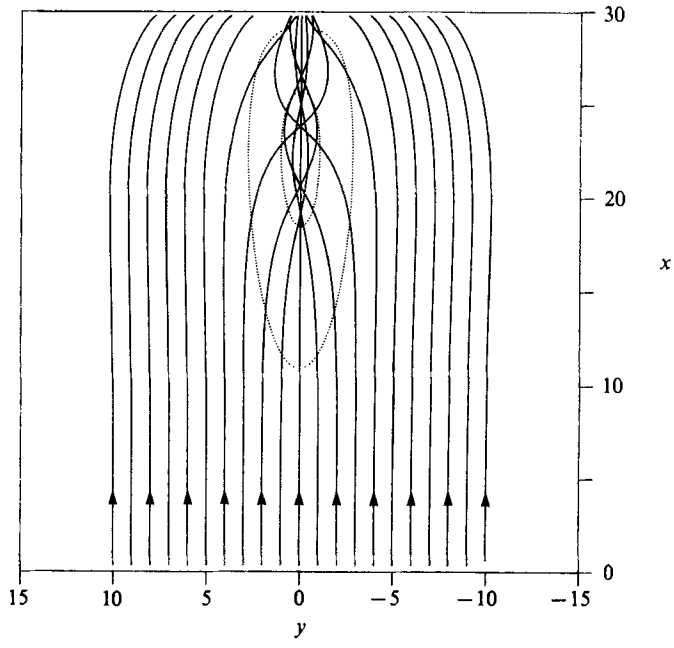

FIGURE 2. Wave ray pattern over rip current with $Fr = 0.2353$, $C_4 = 1.596$ and $C_3 = 7.979$; · · · ·, contour lines of $|U| = |U_{max}|/e^{\frac{1}{2}}$ and $|U_{max}|/e$; ⟶, wave rays.

The Boussinesq equations are still valid and are reduced to linear dispersive wave equations. As waves propagate into shallower water and encounter the current, the nonlinearity grows and the Boussinesq equations are fully utilized.

The water depth along $x' = 0$ is $h_0' = 5.74$ m. Therefore the coastline is located at $x_0' = 287$ m, since the beach slope is 1/50. The dimensionless coastline is $x_0 = 30.0$. The normal incident wave has a wave period of 8 s ($\omega' = 0.785\ \mathrm{s}^{-1}$). The first-harmonic amplitudes, a_0', are 0.0574 m and 0.1148 m along $x = 0$ corresponding to $\epsilon = 0.01$ and 0.02, respectively. Stokes wave theory is used to obtain initial wave amplitudes for higher harmonics.

To illustrate the wave refraction pattern, the wave ray pattern over the current field with $Fr = 0.2353$, $C_4 = 1.596$, $C_3 = 7.979$ is given in figure 2. Noted that the maximum current velocity occurs at $x \approx 22$. It is clear that caustics appear over the current field and the diffraction effects should not be ignored.

Numerical computations were carried out for all six cases listed in table 1 as well as for the linearized problem where only the first harmonic solution ($n = 1$) of (3.13) is obtained without the nonlinear terms. Wave height distributions along different cross-sections are plotted in figure 3 for different cases. Since the centreline of the currents is located at $y = 0$, and along cross-section $y = 15$ the on–offshore current velocity is almost zero, the influence of the current on waves is negligible along $y = 15$; the wave height variations along this cross-section represent the shoaling of incident waves with different initial amplitudes. The shoaling factor, H/H_0, is in general higher for nonlinear waves (larger ϵ-values in figure 3). A snapshot of the free-surface profile along $y = 15$ is shown in figure 4; the nonlinearity increases the sharpness (peakness) of the surface profiles as well as the phase velocity. Numerical computations are stopped when a wave breaking condition, $H/h > 0.8$, is satisfied. At the breaking point the local nonlinearity parameter ϵ takes a value of 0.4, which

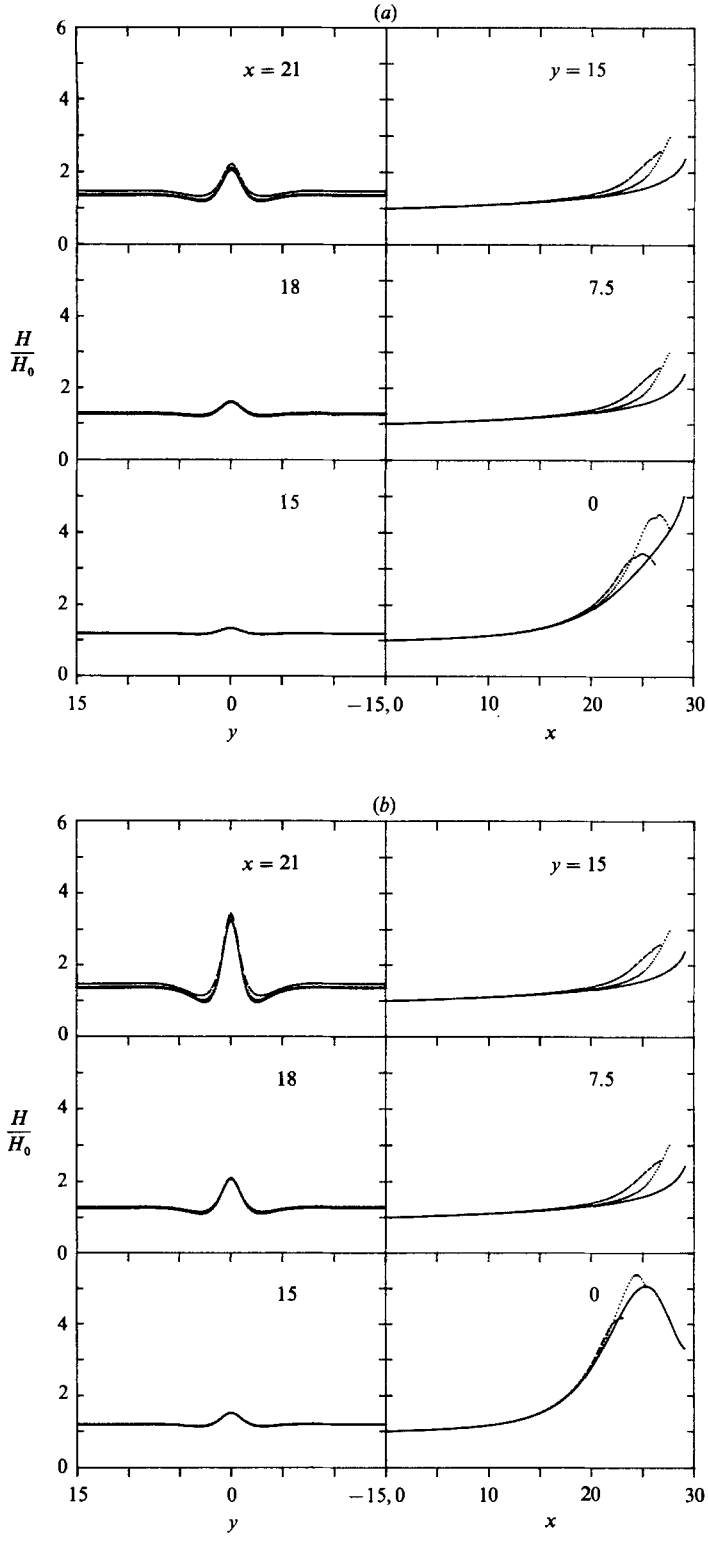

FIGURE 3 (*a*,*b*). For caption see next page.

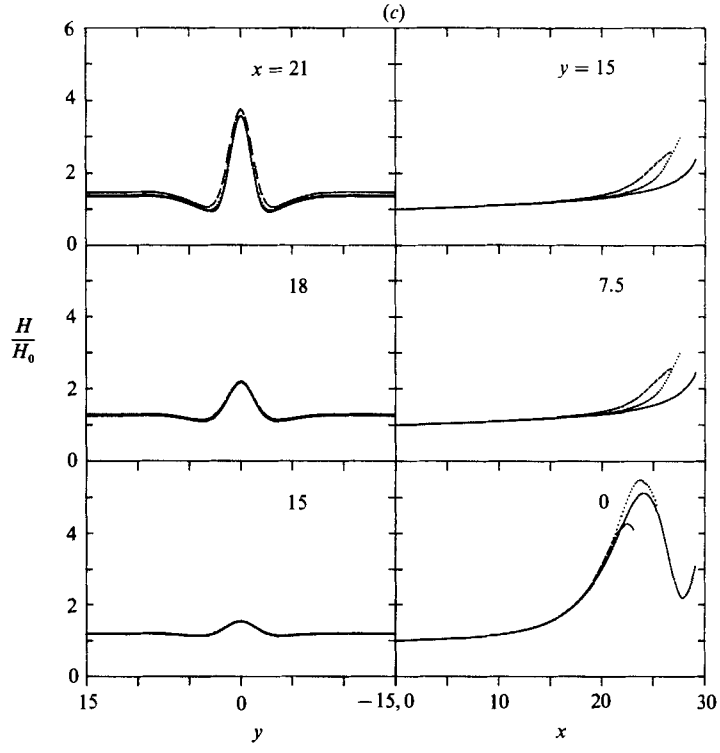

FIGURE 3. Normalized wave height H/H_0 along x = const. (left) and y = const. (right), comparison between linear and nonlinear solutions; ——, linear; · · · ·, $\epsilon = 0.01$; – – –, $\epsilon = 0.02$; for (*a*) $Fr = 0.1177$, $C_4 = 0.798$; (*b*) $Fr = 0.2353$, $C_4 = 0.798$; and (*c*) $Fr = 0.2353$, $C_4 = 1.596$.

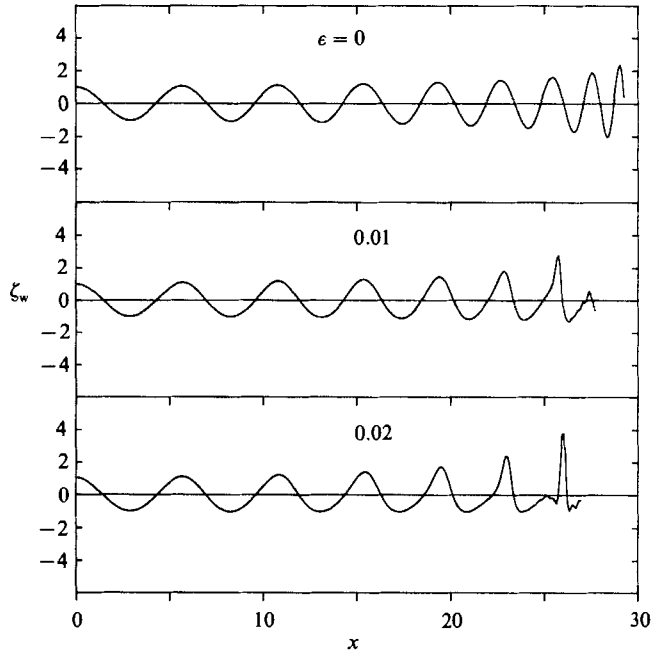

FIGURE 4. Free-surface profile ζ_w along $y = 15$ for the case $Fr = 0.2353$, $C_4 = 0.798$.

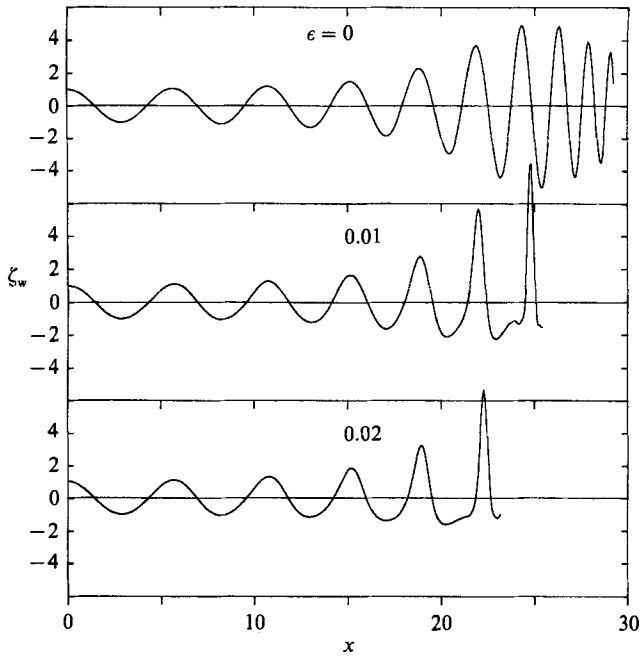

FIGURE 5. Free-surface profile ζ_w along $y = 0$ for the case $Fr = 0.2353$, $C_4 = 0.798$.

is no longer very small. Therefore, strictly speaking, the Boussinesq approximation becomes invalid before the breaking point.

Because of the refraction of incident waves over the currents, waves are focused along the centreline ($y = 0$). Two symmetric shadow regions, roughly along $y = \pm 2.5$, are created, where wave heights are less than the shoaling wave heights (see figure 3). The rapid changes of wave heights in the y-direction confirm the importance of the diffraction. A significant increase in wave heights along $y = 0$ appears as the result of the increase in current velocity. By doubling the on–offshore current width and keeping the same maximum speed, the wave height distributions do not change very much (figure 3*b*, *c*). This is partly because the alongshore (y-direction) velocity component is increased proportionally (see figure 1), which cnhanccs the wave refraction toward the centreline.

For the cases where the Froude number is 0.2352 (figure 3*b*, *c*) the normalized wave heights along the centreline appear to be insensitive to the incident wave heights, up to the breaking point. However, if one examines the free-surface profiles (see figure 5), linear and nonlinear theories give completely different results. This is because the major nonlinear effects are the amplifications of the second harmonics. As long as the first and the second harmonics are in phase, this will not change the wave height but it will increase the wave crests and decrease the wave troughs.

The normalized wave amplitudes for each harmonic are plotted in figure 6 for the cases of $Fr = 0.1177$. Through nonlinearity, wave energy is transferred from the first harmonic to higher harmonics. The rate of energy transfer is higher when the nonlinearity is stronger. As shown in figure 6, the wave amplitudes of the first harmonic for $\epsilon = 0.02$ are smaller than those for $\epsilon = 0.01$. Similar patterns are observed for other cases with different Froude numbers.

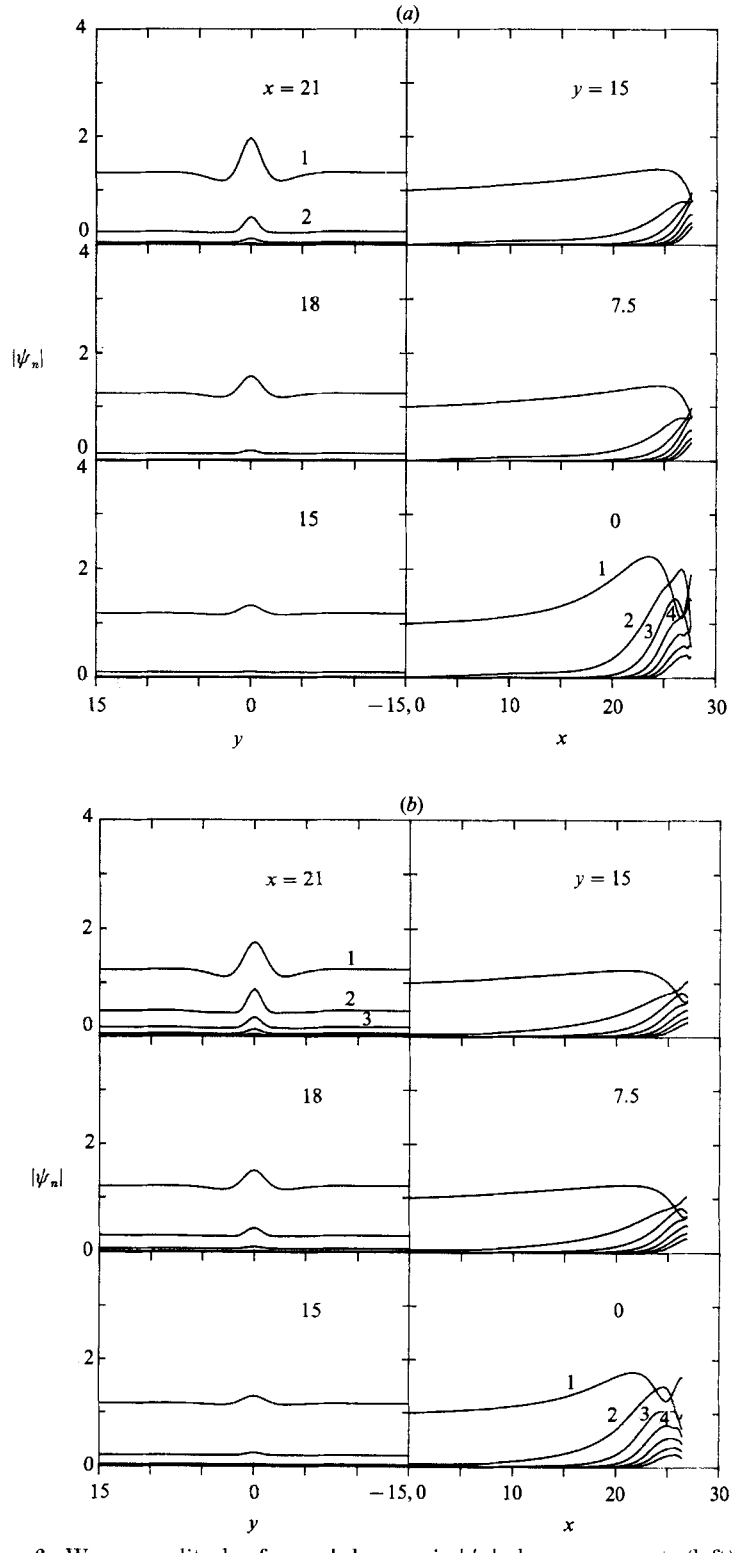

FIGURE 6. Wave amplitudes for each harmonic $|\psi_n|$ along $x = \text{const.}$ (left) and $y = \text{const.}$ (right); $Fr = 0.1177$, $C_4 = 0.798$; (*a*) $\epsilon = 0.01$ and (*b*) $\epsilon = 0.02$.

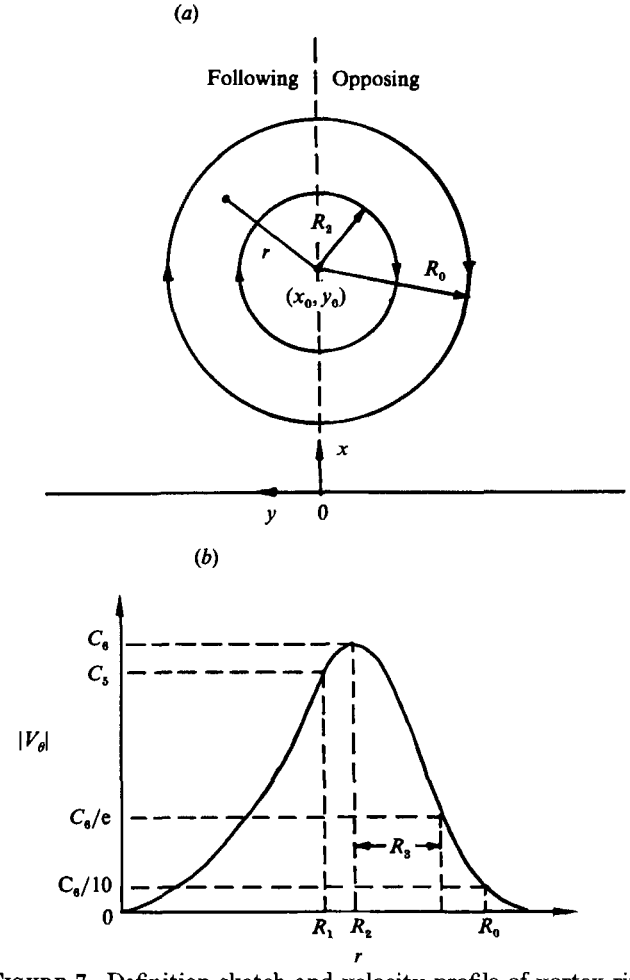

FIGURE 7. Definition sketch and velocity profile of vortex ring.

4.2. *Vortex ring*

The refraction and diffraction of cnoidal waves over an isolated vortex ring is examined here. For a uniform water depth the current velocity and the free-surface displacement in terms of polar coordinates for a vortex ring can be written as (Mapp, Welch & Munday 1985)

$$V_r = 0, \tag{4.6a}$$

$$V_\theta = \begin{cases} C_5\left(\dfrac{r}{R_1}\right)^N, & r \leqslant R_1, \\ C_6 \exp\left[-\left(\dfrac{R_2 - r}{R_3}\right)^2\right], & r > R_1, \end{cases} \tag{4.6b}$$

$$\zeta_c = -\int_r^\infty \frac{V_\theta^2}{r} \mathrm{d}r, \tag{4.6c}$$

where V_r and V_θ are the velocity components in the r- and θ-directions respectively. In (4.6) the constant coefficients C_5, C_6, R_1, R_2, R_3 and N determine the shape and the

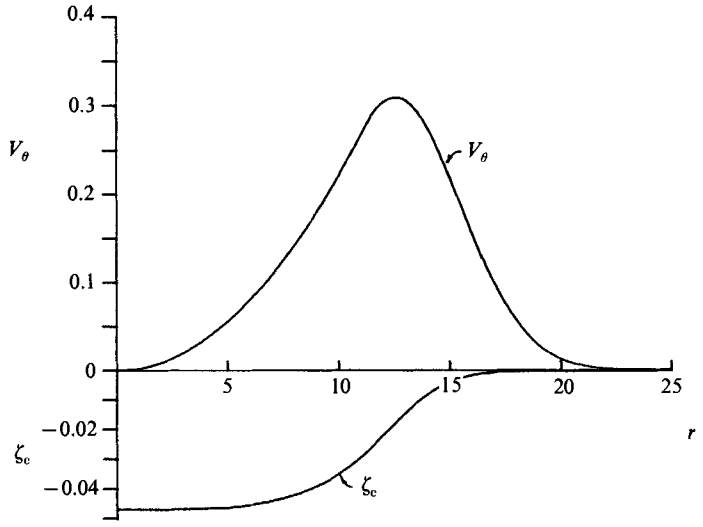

FIGURE 8. Current velocity V_θ and free-surface set-down ζ_c of vortex ring.

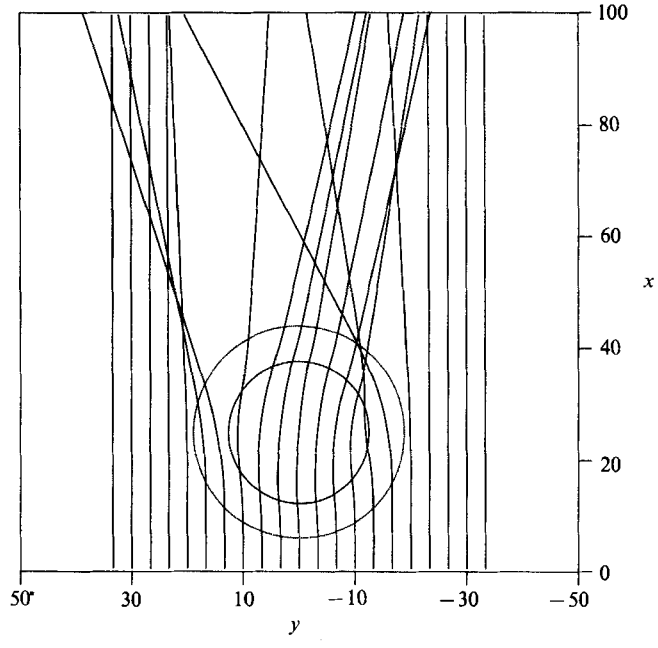

FIGURE 9. Wave ray pattern over vortex ring.

strength of the vortex ring. As shown in figure 7, C_6 represents the maximum speed and R_3 denotes the lengthscale of current variations.

In the present study, a clockwise vortex ring centred at (x_0, y_0) is simulated on a constant water depth. The following numerical data are used for computations:

$$\left.\begin{aligned} &x_0 = 25, \quad y_0 = 0, \quad C_6 = 0.3092, \quad C_5 = 0.9, \\ &R_0 = 6\pi, \quad R_1 = 11.222, \quad R_2 = 4\pi, \quad R_3 = 4.141, \quad N = 2. \end{aligned}\right\} \tag{4.7}$$

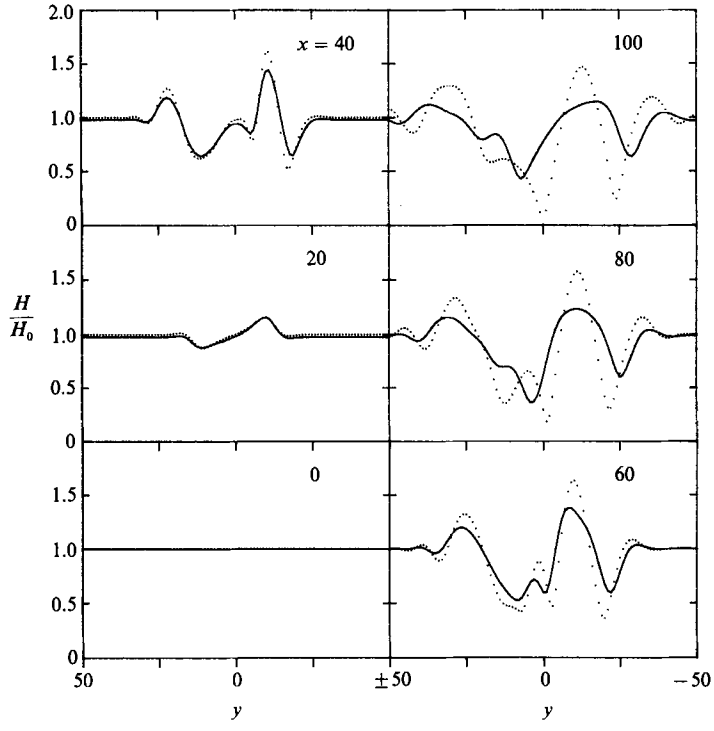

FIGURE 10. Normalized wave height H/H_0 along x = const., comparison between linear and nonlinear solutions; · · · ·, linear; ——, nonlinear.

The current profiles and the corresponding free-surface set-down are shown in figure 8. The incident waves are described by uniform cnoidal waves with wave height $H_0' = 2$ m and wave period, $T' = 19.43$ s. The constant depth is $h_0' = 10$ m. The amplitudes for each harmonic are: $\psi_1' = 0.81701$ m, $\psi_2' = 0.40683$ m, $\psi_3' = 0.16197$ m, $\psi_4' = 0.05756$ m, $\psi_5' = 0.01917$ m, $\psi_6' = 0.00610$ m, $\psi_7' = 0.00186$ m. The corresponding dimensionless parameters ϵ and μ^2 take the values 0.093 and 0.107, respectively.

The wave ray pattern is shown in figure 9. On the left side of the vortex ring waves and currents move in the same direction. Therefore, wave rays diverge. On the other hand, waves and currents move in the opposite directions on the right side of the vortex ring. Consequently, wave rays converge in this neighbourhood. Outside the vortex ring, wave rays remain in straight lines. Wave ray crossings occur behind the vortex ring; a shadow zone is created behind the left side of the vortex ring. The wave ray theory cannot be used to calculate the wave height distribution.

Numerical computations are carried out by solving (3.13). The normalized wave heights along six cross-sections are shown in figure 10. For comparison numerical solutions based on the linearized theory, calculating only the first-harmonic amplitude without nonlinear terms, are also plotted in the figure. The development of the shadow zones and the focal zones is clearly illustrated. In the focal zones the wave heights predicted by the nonlinear theory are lower than those predicted by linear theory. The nonlinearity enhances the diffraction which transfers wave energy in the lateral direction. Wave amplitudes of each harmonic from the nonlinear theory are shown in figure 11 for each cross-section.

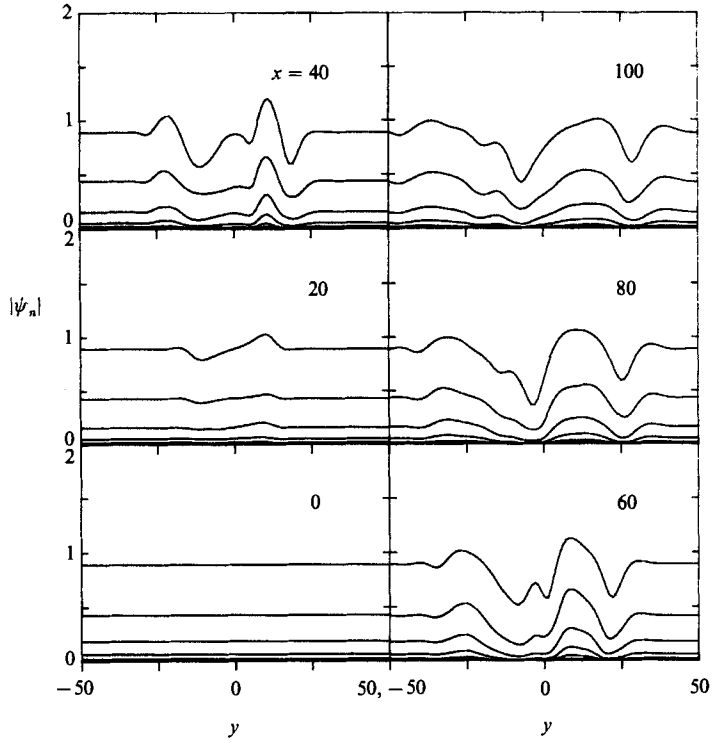

FIGURE 11. Wave amplitudes of each harmonic $|\psi_n|$ along x = const.

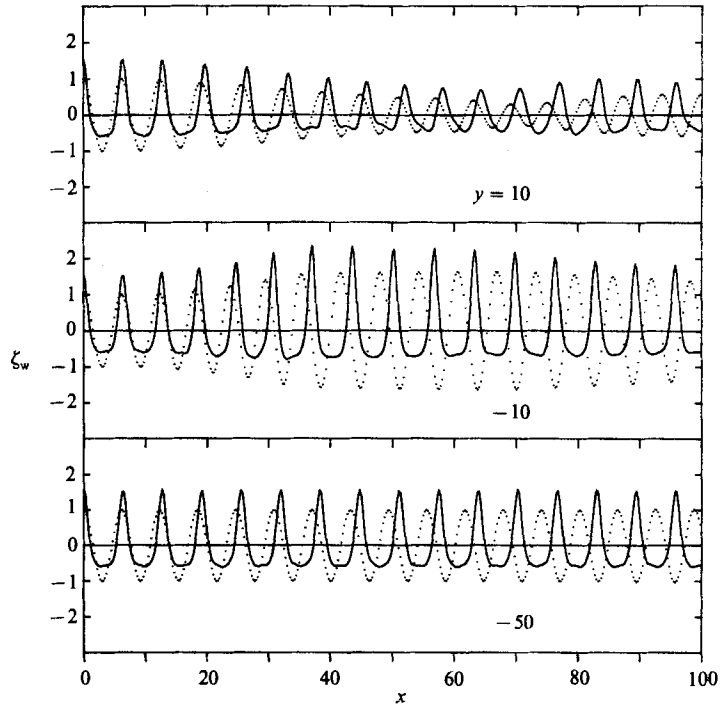

FIGURE 12. Instantaneous free-surface profiles ζ_w along y = const., comparison between linear and nonlinear solutions; · · · ·, linear; ——, nonlinear.

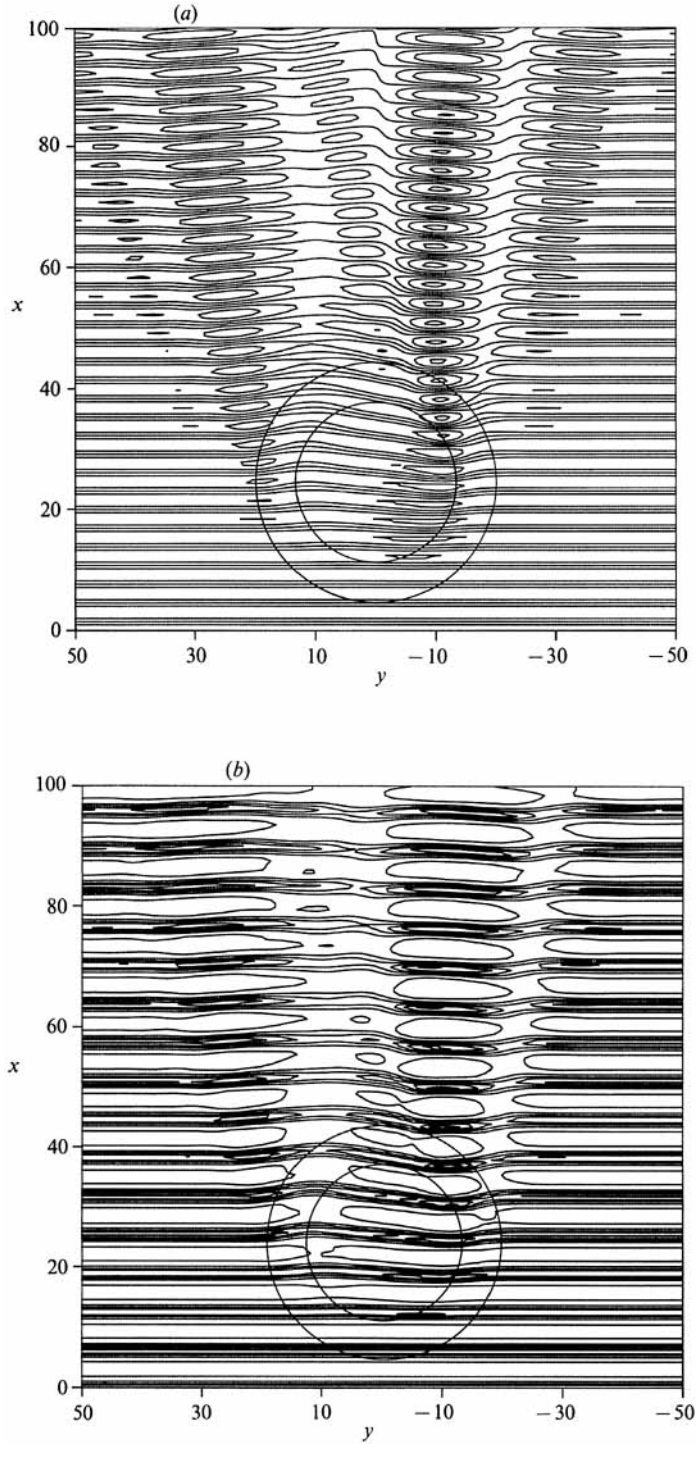

FIGURE 13. Contour plots of instantaneous free-surface displacements over a vortex ring, (*a*) linear theory and (*b*) nonlinear theory.

The instantaneous free-surface profiles along $y = -50$, -10, and 10 are plotted in figure 12. Along $y = -50$ the effects of the current are negligible; the free-surface profiles are the same as those of the incident waves. The cnoidal waves have slightly faster phase speed than the small-amplitude waves. The cross-section $y = -10$ intersects the focal zone. The wave heights are higher than the incident wave heights. The phase speed is slower than that of the incident waves because the currents move in the opposite direction to the wave propagations. Along the cross-section $y = 10$, the amplitudes are small because of the effects of the shadow zone. The phase speeds of both linear and nonlinear waves are faster than those of incident waves since the current velocity is in the same direction as the wave propagation.

The contour plots of the instantaneous free-surface displacements are presented in figure 13 for both linear and nonlinear theories. The increment of contour lines is 0.5. After waves pass the vortex ring, they should recover and become plane waves again. As evident in figure 13, the nonlinear waves recover their plane wave forms faster than the linear waves.

5. Concluding remarks

A new set of Boussinesq equations have been derived in this paper, which can be used to study the full interactions between waves and currents in shallow water. The current velocity is stronger than the wave orbital velocity, but weaker than the phase velocity. The lengthscale of the current variations is longer than the characteristic wavelength. While the horizontal velocity components are nearly uniform throughout the entire depth, the current field is allowed to be rotational.

In computing the wave field, the parabolic approximation has been used. The resulting system of nonlinear parabolic wave equations represents the extension of earlier work by Liu *et al.* (1985), who did not consider currrents. Numerical results for the wave field are obtained with a prescribed current field. Consequently, the full interaction problem is not presented in this paper. However, the present numerical results demonstrate clearly the nonlinear diffraction pattern of shallow-water waves over a shear current.

Yoon (1987) has developed an iterative numerical scheme for solving the full interaction problems. The same solution technique for the wave field as shown in this paper has been used in each iteration step. Although some preliminary results have been reported by Yoon (1987), it is clear that a comparable and efficient numerical scheme for computing the current field is still wanting.

This research was supported by the New York Sea Grant Institute. The manuscript was written when one of us (P.L.F.L.) was visiting the Technical University of Denmark as a Visiting Professor. Discussions with M. W. Dingeman have been very fruitful. Reviewers' comments on an early version of the manuscript are also appreciated.

REFERENCES

ARTHUR, R. S. 1950 Refraction of shallow water waves: the combined effects of currents and underwater topography. *EOS Trans. AGU* **31**, 549–552.

BOOIJ, N. 1981 Gravity waves on water with nonuniform depth and current. *Rep.* 81-1. Dept. of Civil Engrg, Delft University of Technology, Delft.

BRETHERTON, F. P. & GARRETT, C. J. R. 1969 Wave trains in inhomogeneous moving media. *Proc. R. Soc. Lond.* A **302**, 529–554.

KIRBY, J. T. 1984 A note on linear surface wave–current interaction over slowly varying topography. *J. Geophys. Res.* **89**, 745–747.

KIRBY, J. T. 1986 Higher-order approximations in the parabolic equation method for water waves. *J. Geophys. Res.* **91**, 933–952.

LIU, P. L.-F. 1983 Wave–current interaction on a slowly varying topography. *J. Geophys. Res.* **88**, 4421–4426.

LIU, P. L.-F. & MEI, C. C. 1975 Effects of a breakwater on nearshore currents due to breaking waves. *Tech. Mem.* 57. Coastal Engineering Research Center.

LIU, P. L.-F., YOON, S. B. & KIRBY, J. T. 1985 Nonlinear refraction-diffraction of waves in shallow water. *J. Fluid Mech.* **153**, 184–201.

LONGUET-HIGGINS, M. S. & STEWART, R. W. 1960 Changes in form of short gravity waves on long waves and tidal currents. *J. Fluid Mech.* **8**, 565–583.

LONGUET-HIGGINS, M. S. & STEWART, R. W. 1961 The changes in amplitude of short gravity waves on steady non-uniform currents. *J. Fluid Mech.* **10**, 529–549.

MCKEE, W. D. 1974 Waves on a shearing current: a uniformly valid asymptotic solution. *Proc. Camb. Phil. Soc.* **75**, 295–301.

MADSEN, O. S. & MEI, C. C. 1969 Dispersion of long waves of finite amplitude over an uneven bottom. *Rep.* 117. Dept. of Civil Engrg, MIT.

MAPP, G. R., WELCH, C. S. & MUNDAY, J. C. 1985 Wave refraction by warm core rings. *J. Geophys. Res.* **90**, 7153–7162.

PEREGRINE, D. H. 1967 Long waves on a beach. *J. Fluid Mech.* **27**, 815–827.

PEREGRINE, D. H. 1976 Interaction of water waves and currents. *Adv. Appl. Mech.* **16**, 10–117.

PEREGRINE, D. H. & SMITH, R. 1975 Stationary gravity waves on non-uniform free streams. *Math. Proc. Camb. Phil. Soc.* **77**. 415–438.

PHILLIPS, O. M. 1966 *The dynamics of the Upper Ocean.* Cambridge University Press.

SMITH, R. 1976 Giant waves. *J. Fluid Mech.* **77**, 417–431.

YOON, S. B. 1987 Propagation of shallow-water waves over slowly varying depth and currents. Ph.D. thesis, Cornell University, Ithaca, NY.